Article:
Kim, Y, Kim, YK, Kim, JH et al. (3 more authors) (2018) Synthesis of functionalized porous montmorillonite via solid-state NaOH treatment for efficient removal of cesium and strontium ions. Applied Surface Science, 450. pp. 404-412. ISSN 0169-4332

https://doi.org/10.1016/j.apsusc.2018.04.181

Synthesis of functionalized porous montmorillonite via solid-state NaOH treatment for efficient removal of cesium and strontium ions

Yonghwan Kim[a], Yun Kon Kim[a], Jung Hwan Kim[b], Man-SungYim[b], David Harbottle[c] and Jae W. Lee[a]*

[a]Department of Chemical and Biomolecular Engineering, Korea Advanced Institute of Science and Technology (KAIST), Daejeon 305-701, Republic of Korea

[b]Department of Nuclear and Quantum Engineering, Korea Advanced Institute of Science and Technology (KAIST), Daejeon 305-701, Republic of Korea

[c]School of Chemical and Process Engineering, University of Leeds, Leeds LS2 9JT, United Kingdom

Abstract

Solid-state NaOH treatment of montmorillonite clay was used to enhance the removal of Cs^{+} and Sr^{2+}. Through this facile and low-cost modification, montmorillonite with a large BET surface area (117.1 m^2 g^{-1}) and many surface functional groups (Si-O-Na), demonstrated enhanced sorption kinetics (89% removal for 40 mg L^{-1} Cs^{+} and 23 mg L^{-1} Sr^{2+} in 1 h) with a sorption capacity of 290.7 mg g^{-1} for Cs^{+} and 184.8 mg g^{-1} for Sr^{2+}, greatly exceeding the low sorption capacity (137.0 mg g^{-1} for Cs^{+} and 15.6 mg g^{-1} for Sr^{2+}) of pristine montmorillonite. SEM-EDS and XPS analyses revealed that Cs^{+} and Sr^{2+} were ion-exchanged with Na^{+} on the surface functional groups formed following NaOH treatment. The performance of NaOH-treated montmorillonite was stable following gamma-ray irradiation (at 6 Gy h^{-1} for 30 min) and across a broad range of pHs (3 to 11), exhibiting a high distribution coefficient (K_d) of 1.5×10^3 mL g^{-1} for Cs^{+} (1.58 mg L^{-1}) and 3.7×10^3 mL g^{-1} for Sr^{2+} (1.64 mg L^{-1}) under groundwater conditions where various cations including Na^{+}, K^{+}, and Ca^{2+} (V/m = 1 L/g) were present. The proposed method demonstrated great improvement of the sorption capacity of an abundant and inexpensive montmorillonite.

Keywords

Montmorillonite

Alkaline treatment

Cesium

Strontium

Sorption

1. Introduction

Nuclear power remains an attractive energy source as leading nations begin to move away from conventional non-renewables. While nuclear power accounts for a small fraction (~ 9.7%) of the total electricity produced, the treatment of radioactive wastes has become an emerging issue [1,2]. The concern was magnified following the Fukushima nuclear incident in 2011, with the release of radionuclides creating a significant risk, and many countries considering decommissioning their nuclear power plants [3]. Among the radionuclides released, the most radioactive elements are Cs-137 and Sr-90. These radionuclides are fission products of uranium and emit strong gamma rays and beta particles as well as causing long-term damage to ecosystems due to their long half-lives of approximately 30 years, and high mobility in aqueous environments [4–6]. The ion mobility in aqueous environments has generated significant research interest, especially to develop methods to selectively separate the radionuclides from ionic solutions (groundwater, seawater).

To treat radioactive wastewater several methods have been demonstrated such as co-precipitation, evaporation/concentration, chromatography and adsorption/ion-exchange [7]. However, since the target radionuclides, Cs^{+} and Sr^{2+}, coexist in trace amounts in a concentrated solution of competitive cations including Na^{+}, K^{+}, and Ca^{2+}, the sorption method is often desired to process high volumes of wastewater leaving minimal waste for packaging and landfill disposal. Considering the various adsorbents, organic molecular adsorbents [8] or metal hexacyanoferrates [9–13] have shown high selectivity for specific ions such as Cs^{+}. However, due to stability issues of the organic-based materials, there remains a concern about long-term storage of the adsorbent. Titanosilicates [14,15] or metal

sulfides [16,17], which are relatively stable inorganic adsorbents for radiation and heat, have been developed and attracted attention. However, these materials are still being developed for the application of large-capacity treatments due to insufficient ion selectivity or complex production processes.

Alternatively, natural clays are readily abundant and inexpensive, demonstrating reasonable ion exchange capacity [18]. Specifically, montmorillonite clay (MT) having an expandable layered structure has received significant attention owing to its high cation exchange capacity [19,20]. A unit layer of MT is composed of an octahedral AlO_6 sheet sandwiched between two tetrahedral SiO_4 sheets, with numerous exchangeable cations such as Na^+, Mg^{2+}, Ca^{2+}, and Fe^{2+}, existing between the negatively-charged unit layers [18,19,21]. The interlayer spacing is approximately 3.3 Å and can be swelled in aqueous environments [22]. The selective sorption of Cs^+ through the size-sieving effect of the interlayer spacing has been demonstrated, with several attempts to improve separation efficiency by composite formations using carbon, chitosan, or magnetic particles [18,22,23]. Nevertheless, when compared to recently developed sorbents, MT exhibits low capacity and selectivity especially for Sr^{2+}, so it remains difficult to capture both Cs^+ and Sr^{2+}, and currently is less attractive than other sorbents [24,25].

In the current study, microporous montmorillonite with an abundance of sorption sites was prepared by a facile and low-temperature thermal activation using solid-state NaOH. This simple solvent-free process increased the MT sorption capacity for both Cs^+ and Sr^{2+}. Crystallinity, porosity, and functionality of the NaOH-treated MT was controlled by varying

the NaOH concentration in the thermal reaction. The Cs^{+} and Sr^{2+} sorption mechanism of NaOH-treated MT was determined by XPS analysis, with the sorption capacity, sorption kinetics, pH and radiation stability, demonstrated for the NaOH-treated MT.

2. Experimental

2.1. Materials and Methods

Montmorillonite (MT) was purchased from Alfa Aesar and sodium hydroxide (NaOH) obtained from Junsei Chemical. 1.5 g of MT was ground and mixed with solid form of NaOH at different weight ratios of NaOH to MT: 0.5 (NaMT0.5), 1 (NaMT1), and 2 (NaMT2). The mixture was heated to 300 °C (5 °C min^{-1}) and maintained at 300 °C for 1 h under a flow of nitrogen (50 mL min^{-1}). The mixture was then naturally cooled to 130 °C before quenching the system by adding deionized water to the mixture to facilitate the preservation of the Na-functionalized surface [26]. All the sorbents were washed several times with deionized water to remove unreacted NaOH and impurities. Finally the products were dried in an oven at 80 °C.

2.2. Characterization

Scanning Electron Microscopy (SEM, Hitachi SU8230 at 2-5 kV) coupled with an energy dispersive X-ray spectrometer (EDS) was used to characterize the morphology and elemental composition of the prepared samples. High resolution images of the samples were taken using a Transmission Electron Microscope (TEM, JEOL JEM-2100F at 200 kV). Nitrogen adsorption–desorption isotherms at 77 K were measured using a Micromeritics 3 flex after

the samples were degassed under high vacuum at 110 °C for 12 h. The specific surface area was determined by the Brunauer–Emmett–Teller (BET) method. The pore size distribution was determined from a non-local density functional theory (NLDFT) method. X-ray diffraction (XRD) was conducted on a RIGAKU, Smartlab with Kα (l ¼ 0.15406 nm), set at 45 kV and 200 mA. Fourier transform infrared (FT-IR) spectra were measured with an attenuated total reflectance (ATR) crystal on a Nicolet iS50 (400 – 4000 cm^{-1}). X-ray photoelectron spectroscopy (XPS) was performed using a Sigma probe (Thermo VG Scientific) to analyze the chemical bonds. The XPS peaks were fitted using the Avantage software (Thermo VG package), and the binding energy corrected with reference to C 1s at 284.5 eV.

2.3. Sorption experiments

Cs^+ and Sr^{2+} sorption by the prepared sorbents was evaluated using a batch-shaking method. Each powder-form sorbent was immersed in CsCl or $SrCl_2$ aqueous solutions at a sorbent/ solution ratio of 1 g L^{-1}. The mixture was continually agitated at 200 rpm and 25 °C. After a pre-determined time the sorbent was isolated from the sorbate solution using a syringe filter of pore size 0.45 μm. The initial and final ion concentrations were measured using an inductively coupled plasma mass spectrometer (ICP-MS, Agilent ICP-MS 7700S).

Sorption kinetics were determined by immersing (mixed) 20 mg of sorbent in 20 mL of Cs^+ (40 mg L^{-1}) or Sr^{2+} (24 mg L^{-1}) solution for varying times between 10 and 2880 min. At regular time intervals the Cs^+ and Sr^{2+} concentrations were analyzed using ICP-MS. The

sorbed ion quantity, Q_t (mg g^{-1}), and the removal efficiency, RE (%), were determined using the following relationships:

$$Q_t = (C_0 - C_t) \times V/m \quad (1)$$

$$\text{RE} = (C_0 - C_t)/C_0 \times 100\ (\%) \quad (2)$$

where C_0 (mg L^{-1}) is the initial ion concentration, C_t (mg L^{-1}) the ion concentration after time t (min), V (L) the volume of solution, and m (g) the mass of sorbent.

For each prepared sample the sorption isotherm was determined for both Cs^+ and Sr^{2+} by agitating the sorbent in 20 mL solutions of varying concentrations (4 mg L^{-1} and 1000 mg L^{-1}) for 24 h. The solids were then filtered and the final ion concentration (C_e, mg g^{-1}) measured.

The pH stability of NaMT1 was evaluated by immersing 20 mg of NaMT1 in 20 mL solution containing both Cs^+ (14.3 mg L^{-1}) and Sr^{2+} (13.1 mg L^{-1}) at various pHs between pH 2 and 13 for 24 h. HCl and NaOH were used to adjust the pH, and the initial pH of the solution was measured using a S220 digital pH meter (Mettler Toledo). The final ion concentrations were again determined using the previously described method.

Cs^+ and Sr^{2+} selectivity was evaluated by immersing the sorbents in simulated groundwater containing both Cs^+ (1.58 mg L^{-1}) and Sr^{2+} (1.64 mg L^{-1}). 20 mg of the sorbent was added to 20 mL groundwater and shaken for 24 h. The final ion concentrations were measured, and the

removal efficiencies determined using Eq. (2).

3. Results & Discussion

3.1. Textural characterization

The solid phase reaction of MT and NaOH creates micropores via desilication, as illustrated by the proposed mechanism in Fig. 1. The reaction involves deprotonation of surface SiOH groups by NaOH and sequential Si−O bond cleavage [27,28]. The resulting morphology transformation was observed by SEM (Fig. 2). Pristine MT exhibited a plate-like and smooth surface structure as shown in Fig. 2(a). However, the surface progressively roughened by the reaction with NaOH, with the roughness increasing with the ratio of NaOH to MT (Fig. 2(b)-(d)) [28]. In addition, Figs. 2(c) and (d) clearly show the porous structures of NaMT1 and NaMT2, respectively. TEM images of NaOH-treated MTs (Fig. S1) verified the porous surface structures. The observed pore size using TEM appears smaller than a few nanometers.

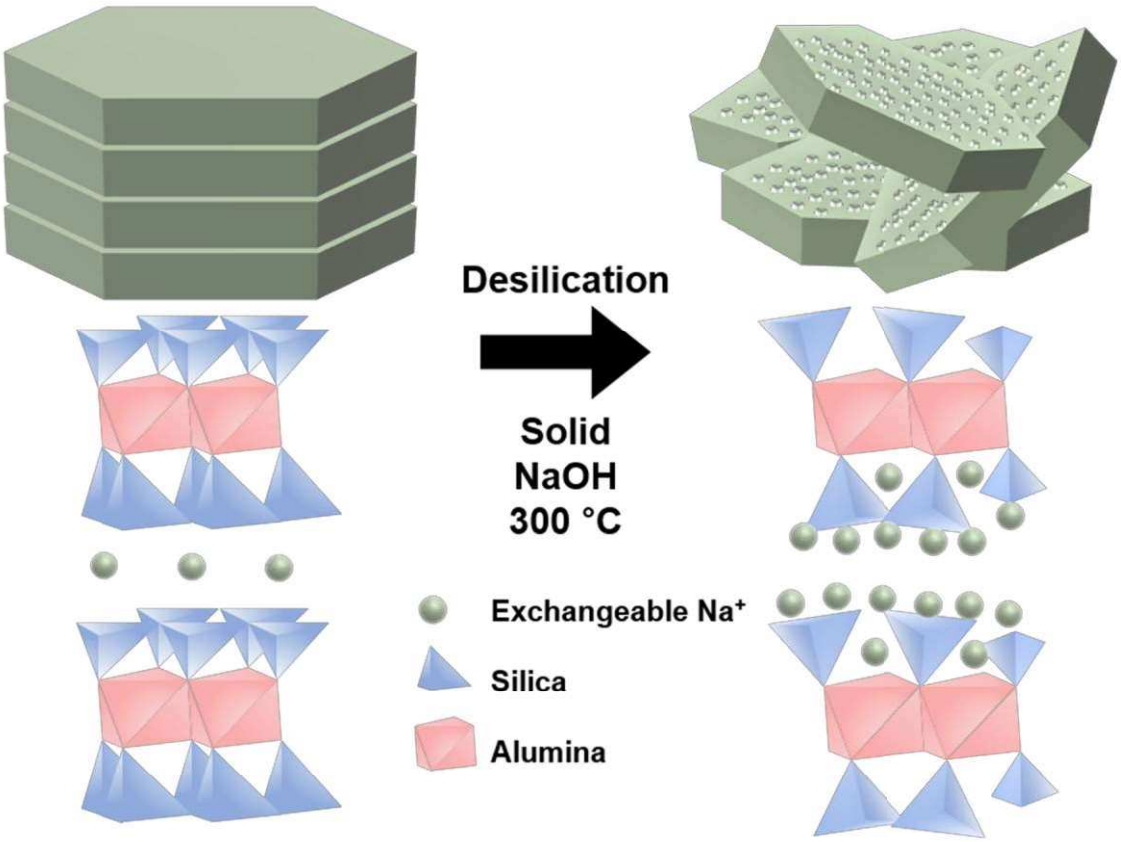

Fig. 1. Representation of NaOH treatment of montmorillonite

The elemental composition of MT following NaOH treatment was determined by SEM-EDS (Table 1). For pristine MT the atomic percentage of Na was 1.76 at%. However, the atomic percentages of Na following the described reaction were approximately 10 at% and almost independent of the NaOH concentration. In addition, the ratio of Si to Al tended to decrease with the increasing NaOH/MT ratio, with the Si/Al ratio being the lowest at 1.26 for NaMT2. SEM imaging and elemental analysis indicated that the silicon was mainly etched away by the base treatment as shown in Fig. 1, therefore it can be speculated that Na^+ predominantly interacts with $Si\text{-}O^-$ through ionic interactions and exists around the etched pores.

Table 1. Composition analysis by SEM-EDS.

Sample	Si/Al	Na/Al	Na at%
MT	2.500	0.217	1.76
NaMT0.5	2.173	1.340	10.08
NaMT1	1.540	0.924	10.20
NaMT2	1.257	0.915	10.45

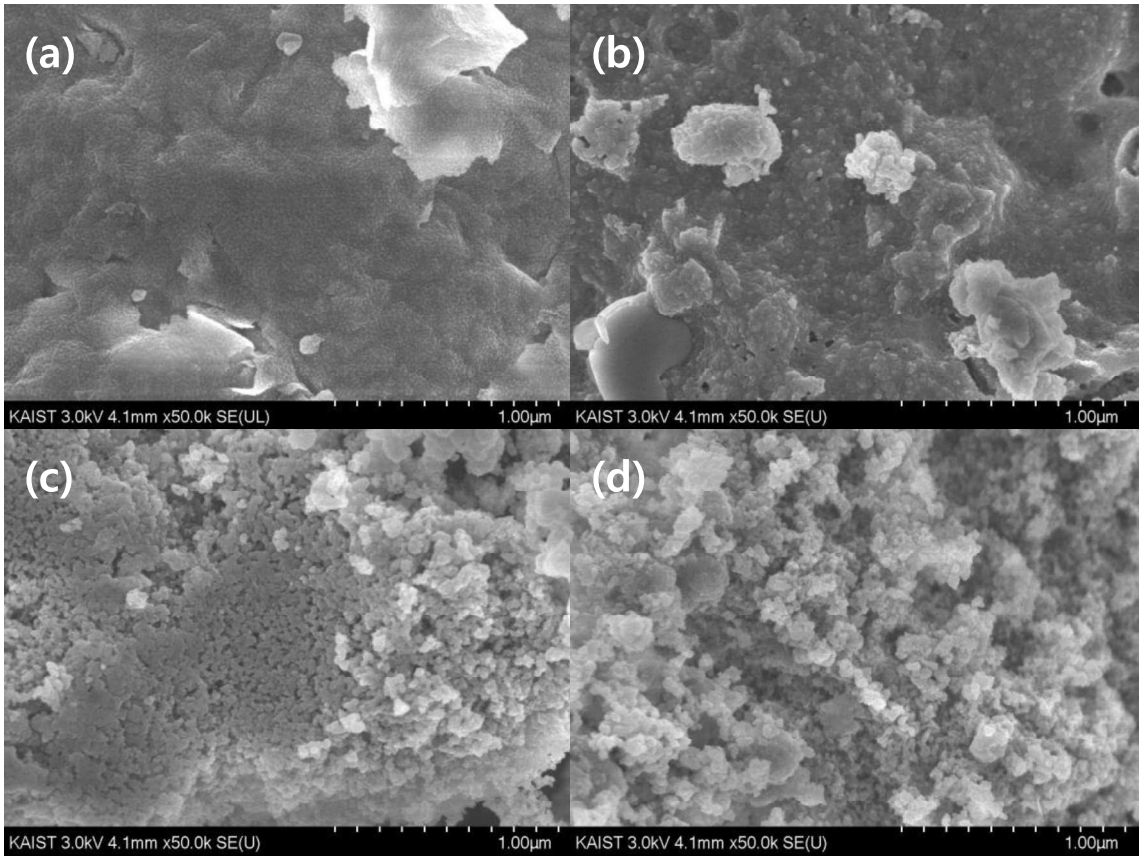

Fig. 2. SEM images of (a) pristine MT, (b) NaMT0.5, (c) NaMT1, and (d) NaMT2.

The porosity of the sorbents was precisely measured by nitrogen adsorption/desorption (Fig. 3(a)). The textural properties such as specific surface area and total pore volume obtained

from N_2 adsorption are summarized in Table 2. The BET surface area of MT was 30.51 $m^2 g^{-1}$ with a total pore volume of 0.093 $cm^3 g^{-1}$, with NaMT0.5 exhibiting a reduced BET surface area (16.55 $m^2 g^{-1}$) and total pore volume (0.069 $cm^3 g^{-1}$), a value slightly lower than MT due to the inadequate activation effect and collapse of interlayer structure of MT following heat treatment. The isotherms of NaMT1 and NaMT2 were distinctly of type IV shape with a sharp uptake of adsorbed N_2 at low relative pressure ($p/p_0 < 0.1$), and an obvious hysteresis loop at higher pressure (0.45 ~1.0 p/p_0). The BET surface areas of NaMT1 and NaMT2 were 117.13 $m^2 g^{-1}$ and 128.99 $m^2 g^{-1}$, respectively, greatly increased when compared to MT. The higher surface area corresponds to the increase in total pore volume with NaMT1 and NaMT2 exhibiting total pore volumes of 0.31 $cm^3 g^{-1}$ and 0.37 $cm^3 g^{-1}$, respectively. The NLDFT pore size distributions confirmed the micro- and mesoporous characteristics of the prepared sorbents (Fig. 3(b)). It is clearly shown that micropores, whose pore widths are smaller than 2 nm, were created in NaMT1 and NaMT2, thus confirming the formation of micropores by the silicon etching process. It can therefore be inferred that sorption sites were created due to the greatly enlarged surface area.

Table 2. N_2 adsorption-desorption.

Sample	**S_{BET} ($m^2 g^{-1}$)**	**V_p ($cm^3 g^{-1}$)**
MT	30.5097	0.093188
NaMT0.5	16.5474	0.069099
NaMT1	117.1306	0.315430
NaMT2	128.9942	0.366995

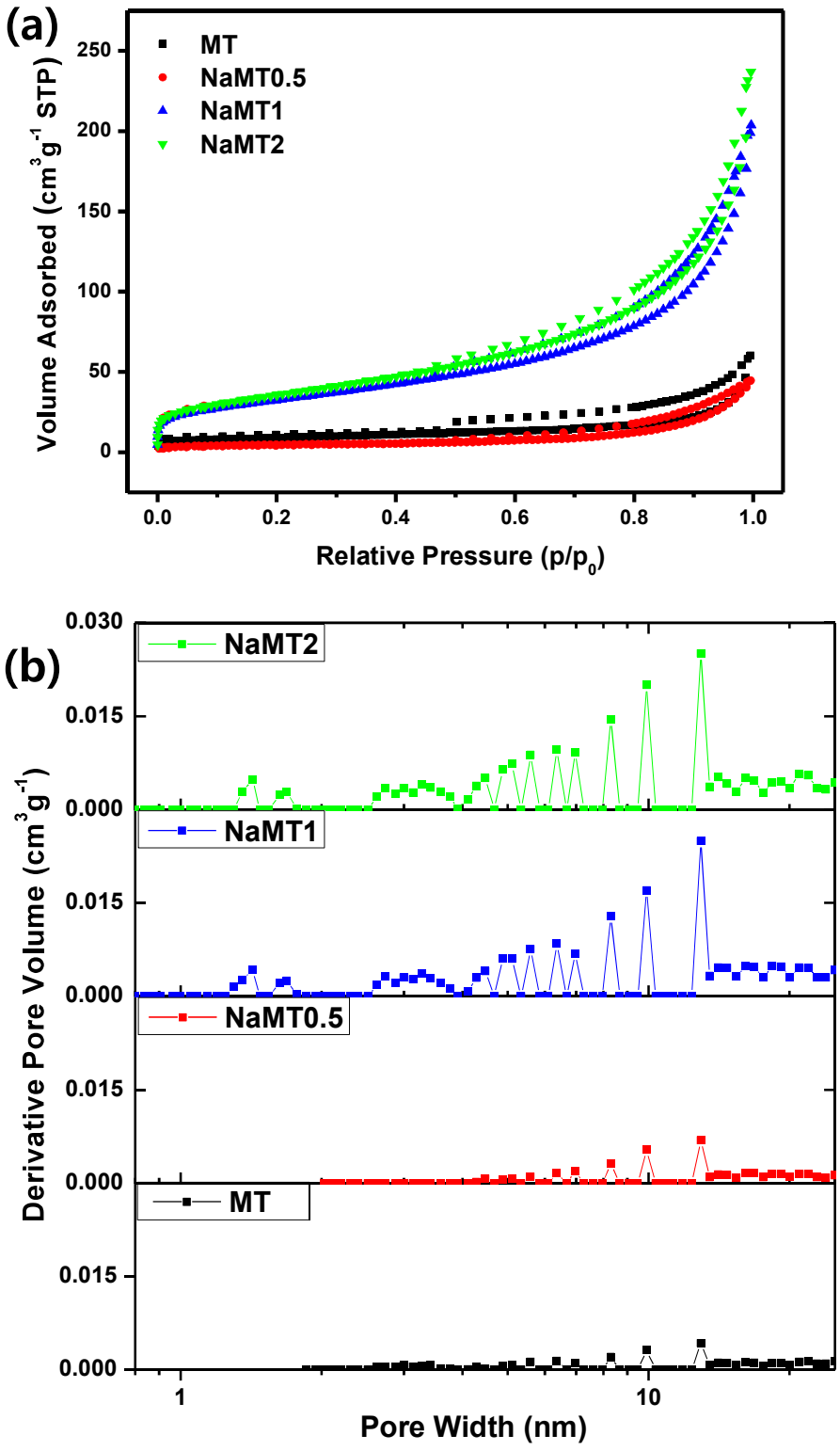

Fig. 3. (a) N_2 adsorption isotherms at 77 K and (b) pore size distributions for MT, NaMT0.5, NaMT1, and NaMT2.

3.2. Chemical characterization

XRD measurements were performed to observe changes in the MT structure following NaOH treatment (Fig. 4(a)). MT exhibited characteristic peaks at 2θ = 6.8°, 8.7°, 19.7°, 20.7°, 21.1°, 27.5°, 34.7°, 39.3°, and 46.2°, in good agreement with the reference peaks of MT (PDF #00-012-0204), and the peaks of quartz at 26.5° and 36.4°. The characteristic peak of the (001) reflection of MT appeared at 6.8°, indicating a basal plane spacing (d_{001}) of 1.29 nm. Considering the thickness of a single MT layer is ~9.6 Å, the interlayer ion-exchangeable spacing is approximately 3.3 Å [18]. However, the (001) peak disappeared following the etching of silicon and excess insertion of Na^+ and surface activation, suggesting layer exfoliation and diminished regularity of the lamellar structure. Also, as the NaOH/MT ratio increased, the overall peak intensities tended to decrease, indicating that the activation process led to an amorphous phase by inducing the desilication and the formation of Si-O-Na functional groups in the clay structure.

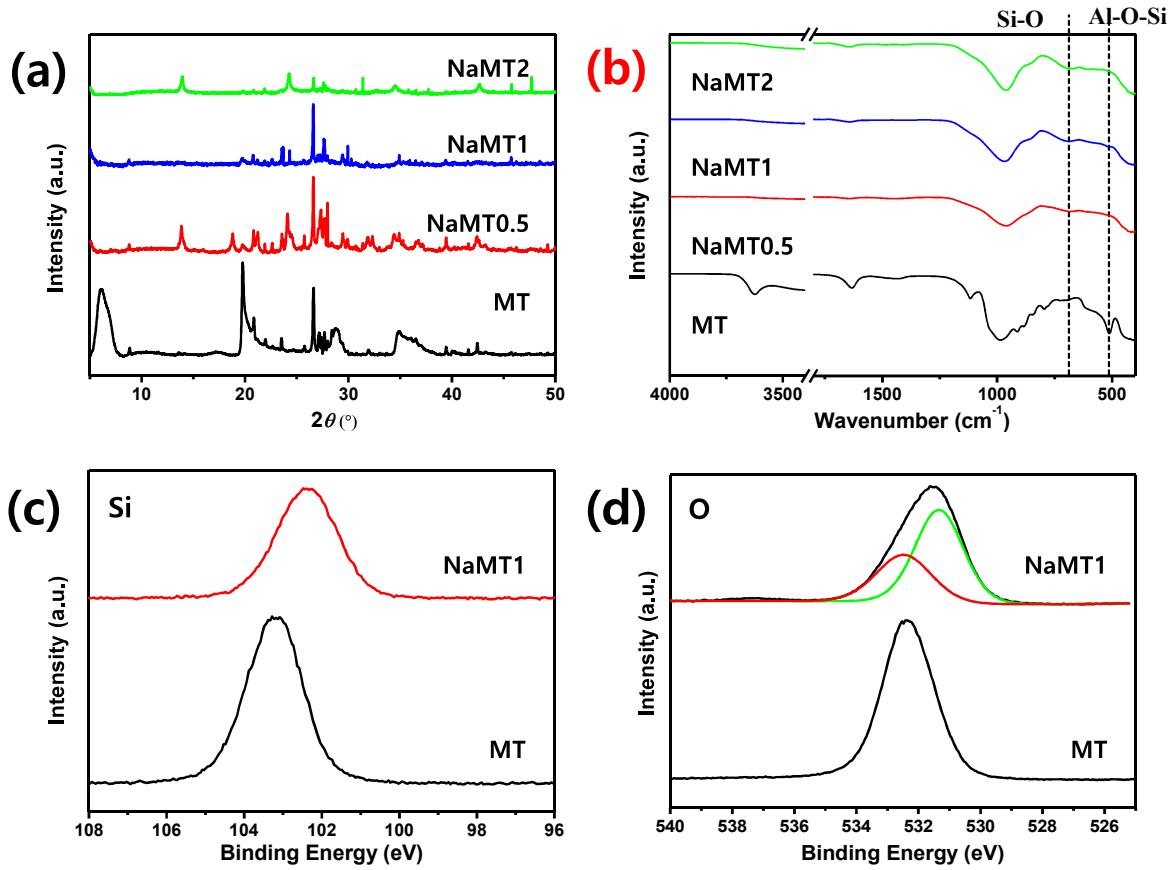

Fig. 4. (a) XRD patterns, (b) FT-IR spectra of MT, NaMT0.5, NaMT1, and NaMT2. XPS spectra of (c) Si 2p peak and (d) O 1s peak for MT and NaMT1.

The functional groups prior to and following the NaOH treatment process were analyzed using FT-IR. Fig. 4(b) shows that MT has characteristic peaks of O-H stretching (3400-3650 cm^{-1}), O-H deformation of water (1632 cm^{-1}), Si-O stretching (1117 cm^{-1} and 985 cm^{-1}), Al-OH-Al deformation (913 cm^{-1}), Si-O stretching of quartz (796 cm^{-1}), Al-O-Si deformation (513 cm^{-1}), and Si-O-Si bending (400 cm^{-1}) [29]. Following NaOH treatment, the peaks at ~ 1630 cm^{-1} and 3400-3600 cm^{-1} diminished owing to dehydration during the high-temperature reaction. In addition, the MT peak at 513 cm^{-1}, which corresponds to Al-O-Si deformation, disappeared following bond cleavage during the reaction with NaOH, and a peak at 685 cm^{-1}

was produced due to the formation of an out-of-plane amorphous Si-O [30]. The data is consistent with the XRD analysis, and it can be deduced that the surface functionality was generated during the base treatment.

XPS was used to validate the effect of desilication on the chemical environment. As shown in Fig. 4(c), the Si 2p core level characteristic peak of NaMT1 (102.4 eV) shifted to a lower energy than that of MT (103.23 eV). The shift relates to the silicon etching process, which reduces the positive cluster SiO_2 in silicon-alumina structures as indicated in zeolite and clay materials [31]. As a result, the Si 2p core level characteristic peak negatively shifted the core electron binding energy of Si element. O 1s characteristic peak of NaMT1 also shifted to a lower energy following NaOH treatment, and it could be clearly deconvoluted into two Gaussian peaks (531.33 eV and 532.47 eV), unlike MT (532.33 eV) (Fig. 4(d)). This result is likely due to the etching effect of positive cluster SiO_2 as seen in the Si 2p spectrum shift, and the formation of surface Al_2O_3 and surface SiO_2 [32]. Considering the MT structure, whose alumina sheet is sandwiched between silica sheets, it is possible to expect that the surface-exposed oxygen functionality has increased as confirmed by FT-IR analysis (Fig. 4(b)).

3.3. Cs^+ and Sr^{2+} Sorption

The sorption equilibrium isotherms were used to compare the prepared sorbents affinity for Cs^+ and Sr^{2+}. The concentration of ions removed was simply determined by measuring the initial and final solution concentrations after 24 h contact. Fig. 5 shows the sorption equilibrium data with isotherms fitted using the well-known non-linear Langmuir equation:

$$Q_e = \frac{Q_m b C_e}{(1 + bC_e)} \quad (3)$$

where Q_e is the adsorbed quantity of Cs^+ and Sr^{2+} (mg g^{-1}) at equilibrium, C_e is the concentration of Cs^+ and Sr^{2+} in the aqueous phase at equilibrium (mg L^{-1}), Q_m is a parameter that represents the maximum sorption capacity (mg g^{-1}), and b is an affinity parameter (L mg^{-1}).

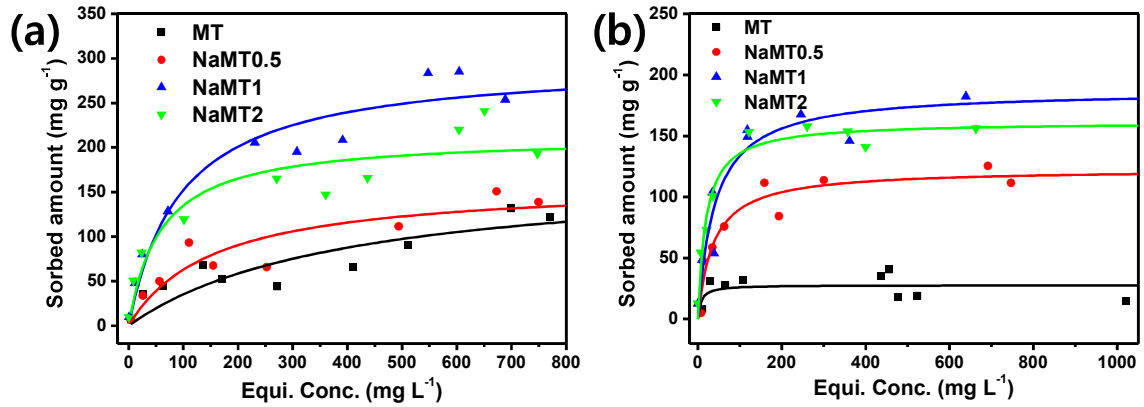

Fig. 5. Sorption isotherms of (a) Cs^+ and (b) Sr^{2+} for MT, NaMT0.5, NaMT1, and NaMT2 with Langmuir fits shown by the solid lines.

As shown in the Fig. 5(a) and Table 3 (the Langmuir isotherm parameters for Cs^+ sorption obtained using a linear regression), MT exhibited the lowest sorption capacity (137.0 mg g^{-1}) and affinity coefficient b (4.74 L g^{-1}) among all prepared sorbents. The NaOH-treated MTs showed largely improved Cs^+ sorption with respect to capacity and affinity, with the sorption capacity increasing in the order of NaMT1 (290.7 mg g^{-1}) > NaMT2 (219.8 mg g^{-1}) > NaMT0.5 (163.1 mg g^{-1}). Also, the sorption equilibrium data for Sr^{2+} indicate that the MT showed poor uptake for Sr^{2+}, most likely relating to the large hydrated ion size of Sr^{2+} (> 4 Å) compared to the interlayer spacing of ~3.3 Å [33]. However, the prepared sorbents (NaMTs)

showed much improved Sr^{2+} capacities, almost equivalent to that of Cs^{+}, with the NaMT1 and NaMT2 samples producing a maximum sorption capacity of 184.8 mg g^{-1} and 156.7 mg g^{-1}, respectively. Therefore, NaOH treatment of MT not only greatly improved the sorption performance for Cs^{+}, but also enabled significant sorption of Sr^{2+}. Moreover, NaMT1 exhibited the high maximum sorption capacity compared to other sorbents (Table 4), presumably a result of the well-generated surface functionality and properly collapsed crystallinity. As such, further sorption analysis was focused on NaMT1.

Table 3. Sorption parameters obtained using the Langmuir equation.

	Cs^{+} sorption			**Sr^{2+} sorption**		
Sorbent	Q_m (mg g^{-1})	b (L g^{-1})	R^2	Q_m (mg g^{-1})	b (L g^{-1})	R^2
MT	136.99	4.741	0.67	15.55	-	0.87
NaMT0.5	163.13	6.358	0.88	129.87	14.52	0.95
NaMT1	290.70	13.040	0.96	184.84	27.10	0.97
NaMT2	219.78	16.132	0.93	156.74	81.50	0.995

Table 4 Cs^{+} and Sr^{2+} sorption capacities for clay-based sorbents.

Target ions	Sorbent	Q_m (mg g^{-1})	Reference
Cs^{+}	Na-treated MT (NaMT1)	290.7	This work
	Chitosan-grafted magnetic MT	160.8	[23]
	Phosphate-modified MT	57.0	[24]
	Ethylamine-modified MT	80.3	[34]
Sr^{2+}	Na-treated MT	184.8	This work
	Phosphate-modified MT	13.3	[24]
	APTES-MT	54.5	[35]
	MnO_2-coated MT	24.6	[36]

The sorption mechanism of NaMT1 and MT was further explored by XPS analysis of samples prepared by mixing 20 mg in either 20 mL of 500 mg/L Cs^{+} or Sr^{2+} for 24 h. As shown in Figs. 6(a) and (b), positions of the Si 2p and O 1s peaks of MT did not shift following sorption, indicating that ion-exchange with interlayer ions did not change the binding energies of the core electrons of Si and O. However, for NaMT1 the binding energies were shifted to lower energies for both Si 2p and O 1s following Cs^{+} sorption (Figs. 6(c) and (d)), since cesium has a lower electronegativity than sodium. In the case of Sr^{2+} exchange with Na^{+} in NaMT1, the electronegativity of strontium is similar to that of sodium, hence the Sr^{2+} sorption did not shift the binding energies of Si and O [37]. Thus for NaMTs, ion exchange occurred via the chemical interaction at the Si-O-Na surface functional groups. Based on the XRD data it was shown that NaMT1 exhibited a higher crystallinity than the more amorphous NaMT2 sample (samples exhibited similar sodium atomic percentages), which may contribute to the enhanced performance (Cs^{+} sorption) of NaMT1, since ion exchange can also occur via the NaMT1 lattice ions.

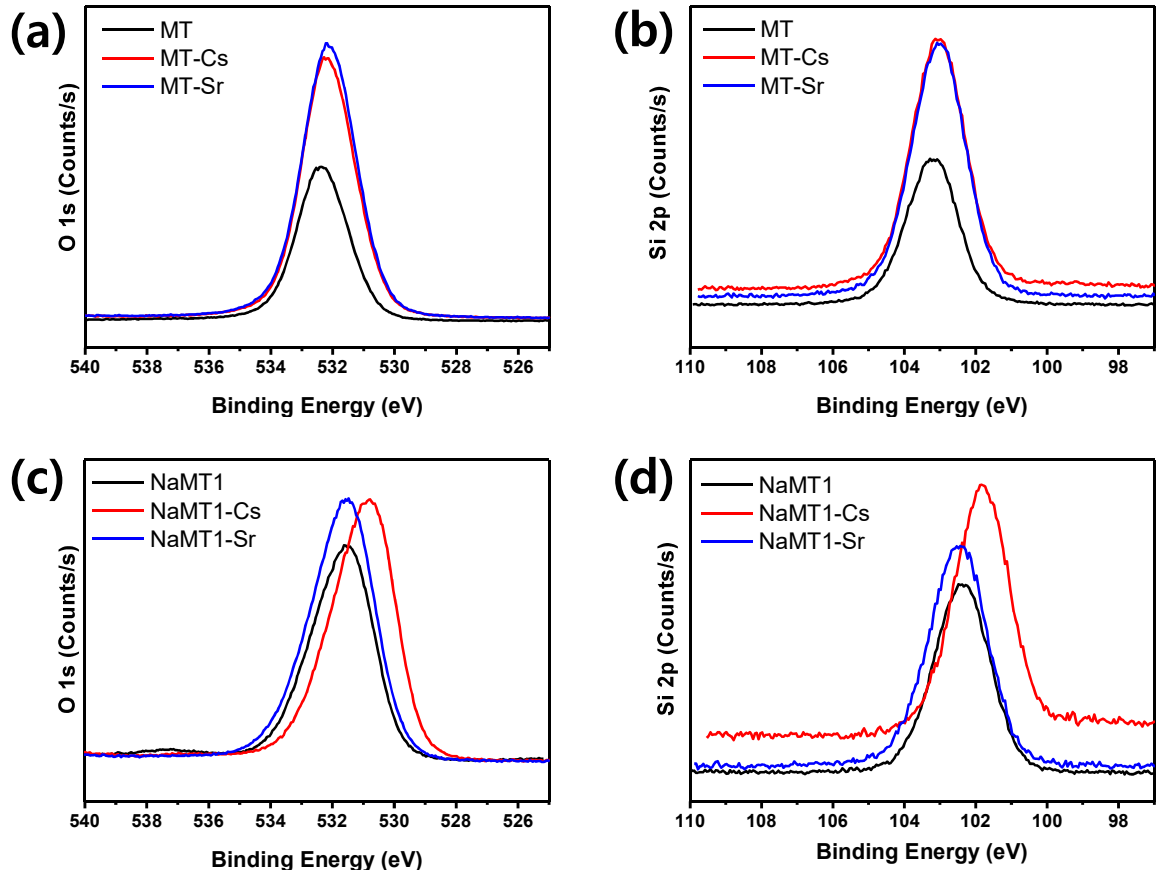

Fig. 6. XPS spectra of (a) O 1s peaks and (b) Si 2p peaks for MT, Cs^{+}-exchanged MT, and Sr^{2+}-exchanged MT, and (c) O 1s peaks and (d) Si 2p peaks for NaMT1, Cs^{+}-exchanged NaMT1, and Sr^{2+}-exchanged NaMT1.

Sorption kinetics were evaluated to determine the removal rates of MT and NaMT1 for Cs^{+} (C_0: 40 mg L^{-1}) and Sr^{2+} (C_0: 24 mg L^{-1}). The data was fitted using a pseudo-second order model, which is often used in chemisorption-based processes to quantify and compare the kinetics of ion-exchange. The linearized model equation is expressed as:

$$\frac{t}{Q_t} = \frac{1}{k_2 Q_e^2} + \frac{t}{Q_e} \quad (4)$$

where Q_t (mg g^{-1}) is the sorbed amount of Cs^{+} or Sr^{2+} at time t (min), Q_e the sorption capacity

at equilibrium (mg g^{-1}), and k_2 (g mg^{-1} min^{-1}) the rate constant parameter. In addition, the initial sorption rate V_0 (mg g^{-1} min^{-1}) was calculated as follows:

$$V_0 = k_2 Q_e^2 \quad (5)$$

Fig. 7 shows the removal efficiency as a function of time, and Table 5 summarizes the kinetic data and fitting parameters. As shown in Fig. 7(a) Cs^+ sorption, pristine MT did not remove all Cs^+ due to insufficient affinity, but NaMT1 removed ~90% in one hour and 98% at equilibrium. For Sr^{2+} removal (Fig. 7(b)), similarly, MT did not remove all Sr^{2+} due to a low affinity, but NaMT1 removed ~90% Sr^{2+} in one hour and approached equilibrium in two hours. NaMT1 showed fast sorption for both Cs^+ and Sr^{2+} thus making the prepared samples useful for practical applications. As shown in Table 5, comparing the initial sorption rates of NaMT1 and MT, the V_0 values of NaMT1 were greater than MT for both Cs^+ and Sr^{2+} sorption. Thus, the sorption rate performance was largely improved along with the ion exchange capacity. Such improvements can be associated to the morphological transition, increasing the material porosity to enhance accessibility of Cs^+ and Sr^{2+} ions to the active sites.

The diffusion-controlled model was also considered to analyze the sorption kinetics by the porous material. The sorption of Cs^+ and Sr^{2+} from solution by the sorbent can be roughly divided into two steps: (i) external and intra-particle diffusion of sorbate and (ii) attachment of the sorbate on the sorbent surface [38]. The intra-particle diffusion model equation is given as:

$$Q_t = k_{id} t^{\frac{1}{2}} + C \quad (6)$$

where k_{id} (mg g^{-1} $min^{-0.5}$) is the diffusion rate constant and C is a constant that represents the thickness of the boundary layer.

Figs. 7(c) and 7(d) show Q_t versus $t^{1/2}$ of MT and NaMT1 for Cs^+ and Sr^{2+} sorption. The data was divided into two parts and fitted using the diffusion-controlled model. The two linear regions represent the multi-stages of the sorption process (external and intra-particle diffusion) which relates to the first linear region, and sorption on the surface interior active sites which relates to the second region. Particularly, for both Cs^+ and Sr^{2+} sorption NaMT1 indicated steeper slopes than those of MT, suggesting the faster intra-particle diffusion of NaMT1 following the NaOH treatment.

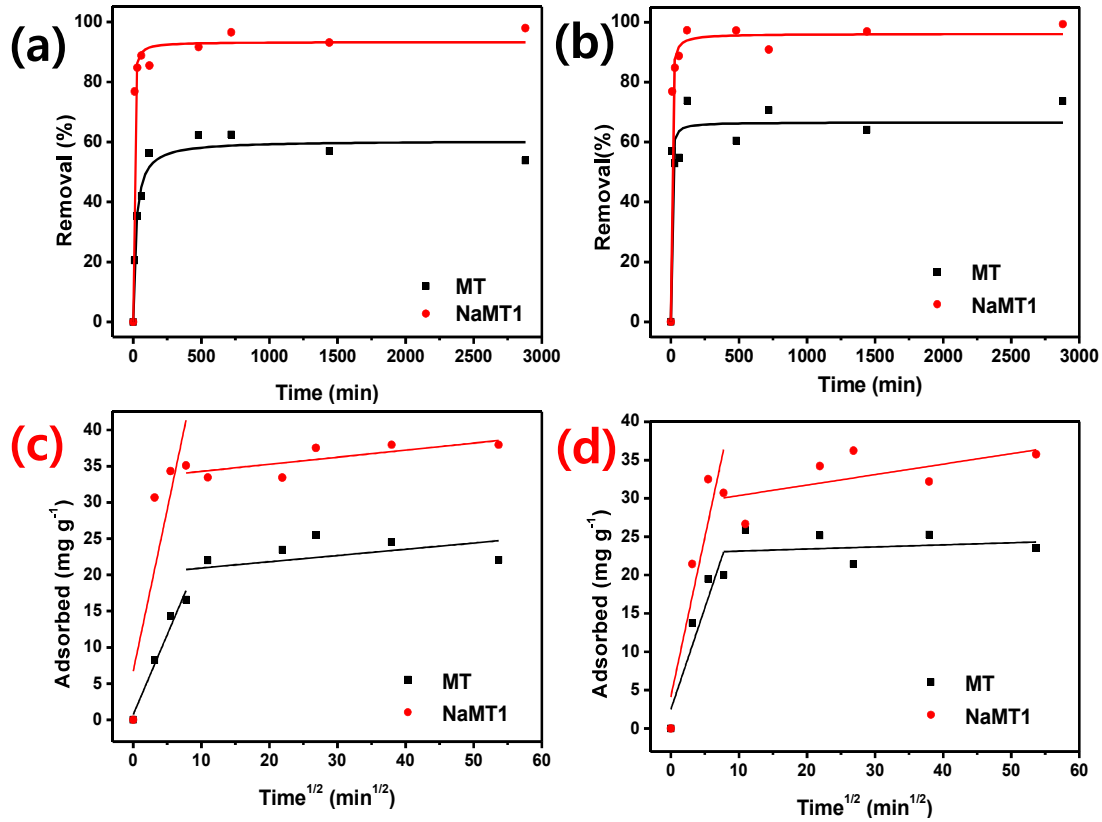

Fig. 7. Uptake kinetics of MT and NaMT1 with fitting curve by pseudo-second order rate equation for (a) Cs^+ and (b) Sr^{2+}, and diffusion-controlled kinetics model for (c) Cs^+ and (b) Sr^{2+}.

Table 5. Pseudo-second order kinetic model parameters for MT and NaMT1.

Sorbent	Cs^+ sorption				Sr^{2+} sorption			
	k_2 ($g mg^{-1} min^{-1}$)	Q_e ($mg g^{-1}$)	V_0 ($mg g^{-1} min^{-1}$)	R^2	k_2 ($g mg^{-1} min^{-1}$)	Q_e ($mg g^{-1}$)	V_0 ($mg g^{-1} min^{-1}$)	R^2
MT	1.91×10^{-3}	24.49	1.15	0.98	5.30×10^{-3}	24.43	3.16	0.95
NaMT1	1.43×10^{-2}	36.30	18.84	0.98	5.72×10^{-3}	33.89	6.57	0.93

The sample stability and sorption performance of NaMT1 was evaluated in different pH conditions. Each solution contained both Cs^+ and Sr^{2+}, and the initial concentrations were 14.3 mg L^{-1} and 13.1 mg L^{-1}, respectively. Greater than 95% of cesium and strontium were removed simultaneously across a broad pH range, pH 3 ~ 11 (Fig. S2). However, sorption significantly diminished in strong acidic conditions (pH 2) due to the interference of H^+. In strongly basic conditions > pH 11, the Cs^+ removal performance diminished, which can be attributed to the competition effect between Na^+ and Cs^+. However, Sr^{2+} removal efficiency remained high, a result of less interference of the monovalent Na^+ with the bivalent Sr^{2+}, but the Sr^{2+} removal efficiency was possibly overestimated due to the precipitation effect of Sr^{2+} in basic conditions [39] .

Studying the sorbent potential to simultaneously remove Cs^+ and Sr^{2+} ions from a realistic solution, the performance was quantified using the distribution coefficient K_d (mL g^{-1}):

$$K_d = \frac{V(C_0 - C_e)}{mC_e} \quad (7)$$

where C_0 and C_e are the initial and equilibrium concentrations of Cs^+ and Sr^{2+} (mg L^{-1}), respectively, V the volume of the sorbate solution (mL), and m the mass of the sorbent (g).

The realistic solution was wastewater simulating groundwater, and the concentrations of competitive ions were: Na^+: ~145 mg L^{-1}, K^+: ~230 mg L^{-1}, Ca^{2+}: ~25 mg L^{-1}. After dissolution of Cs^+ and Sr^{2+} by 1.58 and 1.64 mg L^{-1}, respectively, the sorption results were determined after 24 h. The removal efficiency of MT was less than 20% for both Cs^+ and Sr^{2+} (Table 6), hence, MT did not demonstrate capability to selectively remove trace amounts of target ions. However, NaMT1 and NaMT2 exhibited selective removal efficiency much higher than MT. Specifically, NaMT1 removed ~ 60% of Cs^+ and ~ 80% of Sr^{2+}, with the obtained K_d values given in Table 6 showing a substantially larger selectivity in the order of 10^3. Thus, the simple NaOH treatment not only increases the number of ion-exchangeable sites in the clay structure, but also facilitates selective removal of trace amounts of Cs^+ and Sr^{2+} from a competitive ion-rich environment.

Table 6. Cs^+ and Sr^{2+} removal efficiencies and K_d values from groundwater.

	Cs^+ sorption (C_0: 1.58 mg L^{-1})		**Sr^{2+} sorption** (C_0: 1.64 mg L^{-1})	
Sorbent	Removal (%)	K_d (mL g^{-1})	Removal (%)	K_d (mL g^{-1})
MT	17.84	2.11×10^2	10.12	1.09×10^2
NaMT0.5	37.21	6.11×10^2	40.16	6.92×10^2
NaMT1	60.51	1.52×10^3	79.22	3.77×10^3
NaMT2	53.78	1.16×10^3	86.78	6.53×10^3

To evaluate the sorption performance in radioactive wastewater, the sorbents were exposed to gamma ray radiation, with sorption experiments conducted using irradiated MT and NaMT1 (irradiated using a gamma ray ^{137}Cs source at room temperature (6 Gy h^{-1} for 30 min)). In a prepared solution of Cs^+ (14.9 mg L^{-1}) and Sr^{2+} (15.5 mg L^{-1}), NaMT1 removed 87% of Cs^+ and 92% of Sr^{2+}, with corresponding distribution coefficients in the order of 10^3~10^4, which does not deviate too much from the performance of the non-irradiated NaMT1 (Table 7). Such testing demonstrates that the sorption sites of NaMT1 were not significantly degraded by radiation, highlighting their potential for use in radioactive wastewater.

Table 7. Simultaneous Cs^+ and Sr^{2+} removal efficiencies and K_d values using gamma ray-irradiated sorbents.

	Cs^+ sorption (C_0: 14.89 mg L^{-1})		**Sr^{2+} sorption (C_0: 15.49 mg L^{-1})**	
Sorbent	Removal (%)	K_d (mL g^{-1})	Removal (%)	K_d (mL g^{-1})
MT	17.62	2.20×10^2	52.84	1.15×10^3
NaMT1	86.98	6.68×10^3	92.38	1.21×10^4

4. Conclusions

The ion-exchange capacity of MT for Cs^+ and Sr^{2+} in aqueous solutions was greatly enhanced by the facile solid-state NaOH treatment. Following desilication the crystallinity of MT reduced, while the surface functionality of Si-O-Na increased, producing micropores to form a sample (NaMT1) with a large BET surface area and total pore volume (117.13 m^2/g and 0.315 cm^3 g^{-1}). From the Cs^+ and Sr^{2+} sorption kinetic experiments, NaMT1 exhibited

fast removal performance reaching equilibrium within 1 h. At equilibrium MT exhibited a sorption capacity of 137.0 mg g^{-1} and 15.6 mg g^{-1} for Cs^{+} and Sr^{2+}, respectively. However, following NaOH treatment, NaMT1 exhibited an enhanced sorption capacity of 290.7 mg g^{-1} and 184.8 mg g^{-1} for Cs^{+} and Sr^{2+}, respectively. XPS analyses revealed that the sorbate was exchanged with sodium via chemical interaction at the surface functional sites, which greatly increased the sorption capacity and affinity for Cs^{+} and Sr^{2+}. Moreover, NaMT1 showed excellent pH stability in the range pH 3 to 11, along with radiation stability. Cs^{+} and Sr^{2+} ion removal from groundwater including various dissolved salts was improved compared to MT, demonstrating high specificity for the target ions. The proposed treatment process has been shown to substantially enhance the removal efficiency of Cs^{+} and Sr^{2+}, and due to its simplicity and low cost, is a promising sorbent to decontaminate environments.

Acknowledgement

The authors are grateful for the financial support from the UK-Korea Joint Research Program through NRF grants (NRF-2015M2A7A1000219) funded by the Ministry of Science, ICT and Future Planning. D. Harbottle acknowledges the support of the Engineering and Physical Sciences Research Council grant number EP/M026426/1.

References

[1] Y.K. Kim, Y. Kim, S. Kim, D. Harbottle, J.W. Lee, Solvent-assisted synthesis of potassium copper hexacyanoferrate embedded 3D-interconnected porous hydrogel for highly selective and rapid cesium ion removal, J. Environ. Chem. Eng. 5 (2017) 975–986. doi:10.1016/j.jece.2017.01.026.

[2] H. Yang, H. Li, J. Zhai, L. Sun, Y. Zhao, H. Yu, Magnetic prussian blue/graphene

oxide nanocomposites caged in calcium alginate microbeads for elimination of cesium ions from water and soil, Chem. Eng. J. 246 (2014) 10–19. doi:10.1016/j.cej.2014.02.060.

[3] T.J. Yasunaria, A. Stohl, R.S. Hayano, J.F. Burkhart, S. Eckhardt, T. Yasunarie, Cesium-137 deposition and contamination of Japanese soils due to the Fukushima nuclear accident, Proc. Natl. Acad. Sci. 108 (2011) 19530–19534. doi:10.1073/pnas.1112058108.

[4] M.J. Manos, M.G. Kanatzidis, Layered metal sulfides capture uranium from seawater, J. Am. Chem. Soc. 134 (2012) 16441–16446. doi:10.1021/ja308028n.

[5] Y.K. Kim, T. Kim, Y. Kim, D. Harbottle, J.W. Lee, Highly effective Cs^+ removal by turbidity-free potassium copper hexacyanoferrate-immobilized magnetic hydrogels, J. Hazard. Mater. 340 (2017) 130–139. doi:10.1016/j.jhazmat.2017.06.066.

[6] H. Liu, A. Yonezawa, K. Kumagai, M. Sano, T. Miyake, Cs and Sr removal over highly effective adsorbents ETS-1 and ETS-2, J. Mater. Chem. A. 3 (2015) 1562–1568. doi:10.1039/C4TA06170E.

[7] A. Nilchi, R. Saberi, M. Moradi, H. Azizpour, R. Zarghami, Adsorption of cesium on copper hexacyanoferrate-PAN composite ion exchanger from aqueous solution, Chem. Eng. J. 172 (2011) 572–580. doi:10.1016/j.cej.2011.06.011.

[8] Z. Wu, M. Wang, X. An, J. Du, H. Fan, N. Lin, et al., Intelligent nanospheres with potential-triggered undamaged regeneration ability and superparamagnetism for selective separation of cesium ion, Chem. Eng. J. 325 (2017) 229–238. doi:10.1016/j.cej.2017.05.006.

[9] Y. Kim, Y.K. Kim, S. Kim, D. Harbottle, J.W. Lee, Nanostructured potassium copper hexacyanoferrate-cellulose hydrogel for selective and rapid cesium adsorption, Chem. Eng. J. 313 (2016) 1042–1050. doi:10.1016/j.cej.2016.10.136.

[10] T. Vincent, C. Vincent, E. Guibal, Immobilization of metal hexacyanoferrate ion-exchangers for the synthesis of metal ion sorbents - A mini-review, Molecules. 20 (2015) 20582–20613. doi:10.3390/molecules201119718.

[11] T. Vincent, C. Vincent, Y. Barré, Y. Guari, G. Le Saout, E. Guibal, Immobilization of metal hexacyanoferrates in chitin beads for cesium sorption: synthesis and characterization, J. Mater. Chem. A. 2 (2014) 10007. doi:10.1039/c4ta01128g.

[12] A.A. Kadam, J. Jang, D.S. Lee, Facile synthesis of pectin-stabilized magnetic graphene oxide Prussian blue nanocomposites for selective cesium removal from aqueous solution, Bioresour. Technol. 216 (2016) 391–398. doi:10.1016/j.biortech.2016.05.103.

[13] Lalhmunsiama, C. Lalhriatpuia, D. Tiwari, S.M. Lee, Immobilized nickel hexacyanoferrate on activated carbons for efficient attenuation of radio toxic Cs(I) from aqueous solutions, Appl. Surf. Sci. 321 (2014) 275–282. doi:10.1016/j.apsusc.2014.09.200.

[14] A. Dyer, M. Pillinger, S. Amin, Ion exchange of caesium and strontium on a

titanosilicate analogue of the mineral pharmacosiderite, J. Mater. Chem. 9 (1999) 2481–2487. doi:Doi 10.1039/A905549e.

[15] O. Oleksiienko, C. Wolkersdorfer, M. Sillanpää, Titanosilicates in cation adsorption and cation exchange – A review, Chem. Eng. J. 317 (2017) 570–585. doi:10.1016/j.cej.2017.02.079.

[16] M.J. Manos, M.G. Kanatzidis, Highly Efficient and Rapid Cs^+ Uptake by the Layered Metal Sulfide $K_{2x}Mn_xSn_{3-x}S_6$ (KMS-1), J. Am. Chem. Soc. 131 (2009) 6599–6607. doi:10.1021/ja900977p.

[17] J.L. Mertz, Z.H. Fard, C.D. Malliakas, M.J. Manos, M.G. Kanatzidis, Selective removal of Cs^+, Sr^{2+}, and Ni^{2+} by $K_{2x}Mg_xSn_{3-x}S_6$ (x = 0.5-1) (KMS-2) relevant to nuclear waste remediation, Chem. Mater. 25 (2013) 2116–2127. doi:10.1021/cm400699r.

[18] L. Chen, C.H. Zhou, S. Fiore, D.S. Tong, H. Zhang, C.S. Li, et al., Functional magnetic nanoparticle/clay mineral nanocomposites: Preparation, magnetism and versatile applications, Appl. Clay Sci. 127–128 (2016) 143–163. doi:10.1016/j.clay.2016.04.009.

[19] H. Zhang, Y.K. Kim, T.N. Hunter, A.P. Brown, J.W. Lee, D. Harbottle, Organically modified clay with potassium copper hexacyanoferrate for enhanced Cs^+ adsorption capacity and selective recovery by flotation, J. Mater. Chem. A. 5 (2017) 15130–15143. doi:10.1039/C7TA03873A.

[20] D. Qin, X. Niu, M. Qiao, G. Liu, H. Li, Z. Meng, Adsorption of ferrous ions onto montmorillonites, Appl. Surf. Sci. 333 (2015) 170–177. doi:10.1016/j.apsusc.2015.02.019.

[21] D.A. Almasri, T. Rhadfi, M.A. Atieh, G. McKay, S. Ahzi, High performance hydroxyiron modified montmorillonite nanoclay adsorbent for arsenite removal, Chem. Eng. J. 335 (2018) 1–12. doi:10.1016/j.cej.2017.10.031.

[22] K. Peng, H. Yang, Carbon hybridized montmorillonite nanosheets: preparation, structural evolution and enhanced adsorption performance, Chem. Commun. 53 (2017) 6085–6088. doi:10.1039/C7CC02334K.

[23] S. Yang, N. Okada, M. Nagatsu, The highly effective removal of Cs^+ by low turbidity chitosan-grafted magnetic bentonite, J. Hazard. Mater. 301 (2016) 8–16. doi:10.1016/j.jhazmat.2015.08.033.

[24] B. Ma, S. Oh, W.S. Shin, S.J. Choi, Removal of Co^{2+}, Sr^{2+} and Cs^+ from aqueous solution by phosphate-modified montmorillonite (PMM), Desalination. 276 (2011) 336–346. doi:10.1016/j.desal.2011.03.072.

[25] S. Baik, H. Zhang, Y.K. Kim, D. Harbottle, J.W. Lee, Enhanced adsorption capacity and selectivity towards strontium ions in aqueous systems by sulfonation of CO_2 derived porous carbon, RSC Adv. 7 (2017) 54546–54553. doi:10.1039/C7RA09541D.

[26] C. Ning, M. Xu, D. Chi-Wai HUI, C. LIN Sze Ki, G. McKay, Study of Quench Effect on Heavy Metal Uptake Efficiency by an Aluminosilicate-based Material, Chem. Eng.

J. 311 (2016) 37–45. doi:10.1016/j.cej.2016.11.078.

[27] D. Zhai, L. Zhao, Y. Liu, J. Xu, B. Shen, J. Gao, Dissolution and absorption: A molecular mechanism of mesopore formation in alkaline treatment of zeolite, Chem. Mater. 27 (2015) 67–74. doi:10.1021/cm503151k.

[28] Y. Zhao, Q. Hao, Y. Song, W. Fan, Z. Liu, Z. Liu, Cobalt Supported on Alkaline-Activated Montmorillonite as an E ffi cient Catalyst for Fischer − Tropsch Synthesis, Energy & Fuels. 27 (2013) 6362–6371. doi:10.1021/ef401291q.

[29] S.U. Adikary, D.D. Wanasinghe, Characterization of locally available Montmorillonite clay using FTIR technique, Annu. Trans. Inst. Eng. Sri Lanka2. 1 (2012) 140–145.

[30] M. Hayati-Ashtiani, Characterization of nano-porous bentonite (Montmorillonite) particles using FTIR and BET-BJH analyses, Part. Part. Syst. Charact. 28 (2012) 71–76. doi:10.1002/ppsc.201100030.

[31] T.L. Barr, M.A. Lishka, ESCA Studies of the Surface Chemistry of Zeolites, J. Am. Chem. Soc. 108 (1986) 3178–3186. doi:10.1021/ja00272a004.

[32] W. Gruenert, M. Muhler, K.-P. Schroeder, J. Sauer, R. Schloegl, Investigations of Zeolites by Photoelectron and Ion Scattering Spectroscopy. 2. A New Interpretation of XPS Binding Energy Shifts in Zeolites, J. Phys. Chem. 98 (1994) 10920–10929. doi:10.1021/j100093a039.

[33] E.R. Nightingale, Phenomenological Theory of Ion Solvation. Effective Radii of Hydrated Ions, J. Phys. Chem. 63 (1959) 1381–1387. doi:10.1021/j150579a011.

[34] H. Long, P. Wu, N. Zhu, Evaluation of Cs+ removal from aqueous solution by adsorption on ethylamine-modified montmorillonite, Chem. Eng. J. 225 (2013) 237–244. doi:10.1016/j.cej.2013.03.088.

[35] P. Wu, Y. Dai, H. Long, N. Zhu, P. Li, J. Wu, et al., Characterization of organo-montmorillonites and comparison for Sr(II) removal: Equilibrium and kinetic studies, Chem. Eng. J. 191 (2012) 288–296. doi:10.1016/j.cej.2012.03.017.

[36] Y. Park, W.S. Shin, S.J. Choi, Sorptive removal of cobalt, strontium and cesium onto manganese and iron oxide-coated montmorillonite from groundwater, J. Radioanal. Nucl. Chem. 291 (2012) 837–852. doi:10.1007/s10967-011-1527-7.

[37] W. Gordy, W.J.O. Thomas, Electronegativities of the Elements, J. Chem. Phys. 24 (1956) 439–444. doi:10.1063/1.1742493.

[38] N. Li, R. Bai, Copper adsorption on chitosan-cellulose hydrogel beads: Behaviors and mechanisms, Sep. Purif. Technol. 42 (2005) 237–247. doi:10.1016/j.seppur.2004.08.002.

[39] E.A. Behrens, A. Clearfield, Titanium silicates, $M_3HTi_4O_4(SiO_4)_3 \cdot 4H_2O$ ($M=Na^+$, K^+),with three-dimensional tunnel structures for the selective removal of strontium and cesium from wastewater solutions, Microporous Mater. 11 (1997) 65–75. doi:10.1016/S0927-6513(97)00022-9.